FIRST YEAR PERFORMANCE OF THE TPS BOOSTER RING

H. J. Tsai†, P. J. Chou, K. H. Hu, K. T. Hsu, C.C. Kuo,
C. Y. Liao, Y. C. Liu, G. H. Luo, F. H. Tseng
National Synchrotron Radiation Research Center, Hsinchu 30076, Taiwan

Abstract

The Taiwan Photon Source (TPS) is a 3-GeV low-emittance light source of circumference 518.4 m. The booster ring is in the same tunnel with the storage ring; its circumference at 496.8 m makes it the largest booster ring in operation in existing light sources. Since the successful commissioning at the end of 2014, the TPS booster ring has been optimized in performance for routine operation. In this paper, we present the system upgrade and the improvement of the ramping procedure to increase the capture and ramping efficiency of the beam charge, the characterization of the optics, etc.

INTRODUCTION

The TPS booster ring and storage ring were successfully commissioned in 2014 December [1,2]. Further commissioning with a superconducting RF system and insertion devices took place in the second half of 2015 [3]. The TPS booster ring was designed to share the same tunnel with the storage ring (see Fig. 1). The access to booster was constrained during the commissioning of storage ring. However, we still have great improvement in the capture and ramping efficiency with the following actions: (1) a new working tune and smaller vertical orbit distortion, (2) a real-time power-supply compensation scheme to eliminate the long-term drift of quadrupoles driving current, and (3) an optimized RF synchrotron station phase to match the LINAC working condition. We report also measurements of the longitudinal beam motion and emittance evolution during booster beam ramping.

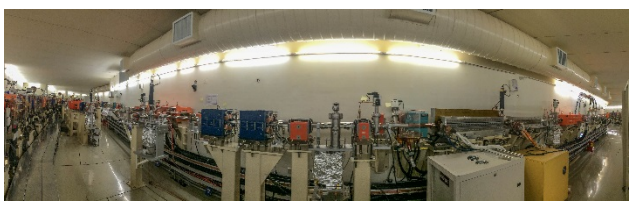

Figure 1: TPS booster ring and storage ring in the same tunnel, as shown in the booster extraction area.

STABILITY OF POWER SUPPLY AND RF STATION PHASE

The reproducibility of the ramping power supplies was target to ±0.25 % with respect to injection energy at 150 MeV. In particular, the variation of the QF power supply causes an unacceptable tune change, i.e., $\Delta\nu_x/\Delta I$=5 (I_{QF}=3.5A) at 150 MeV. Real-time modifications of the power-supply waveform must be implemented to improve the capture and ramping efficiency. Figure 2 displays a histogram of the booster quadrupoles with and without correction. The most of quadrupoles show smaller variations after offset corrections. The booster beam current at 3 GeV before and after correction is shown in Figure 3.

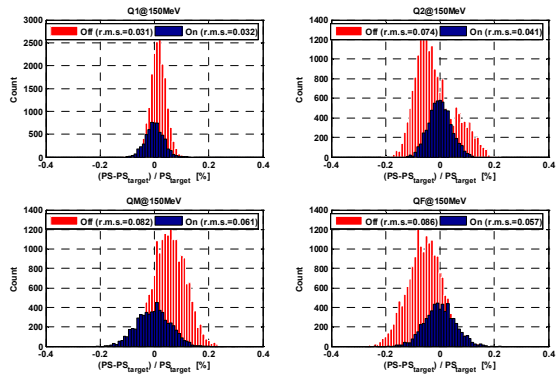

Figure 2: Histogram of booster quadrupoles with and without correction.

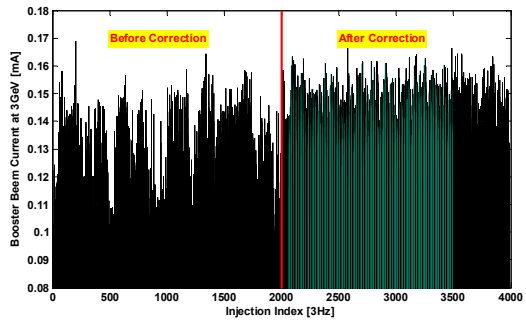

Figure 3: Comparison of booster beam current at 3GeV for the case of before and after offset correction.

There are three bunches, one major central bunch and two smaller side bunches from the 3-GHz LINAC to inject into 500 MHz booster's RF bucket. As the arrival time of bunches changes as shown in Figure 4, which giving indication of the RF synchrotron station phase must be chosen at an insensitive point. The small physical transverse acceptance of the TPS booster ring requires stringent requirements on the LINAC beam quality. The longitudinal beam motion, ~300 turns, at the beginning of ramping and the booster beam current at 3 GeV due to varied RF synchrotron phase setting are shown in Figure 4. The intensive of the extraction beam current improved after optimization.

Taking the actions mentioned above, we can obtain much improved performance in routine operation. So far,

† jacky@nsrrc.org.tw

the beam current during booster routine operation is about 0.16 mA. The overall efficiency of transmission is above 80 % from 150 MeV to 3 GeV. The FCT beam transmission of the TPS booster ring during ramping is shown in Figure 5.

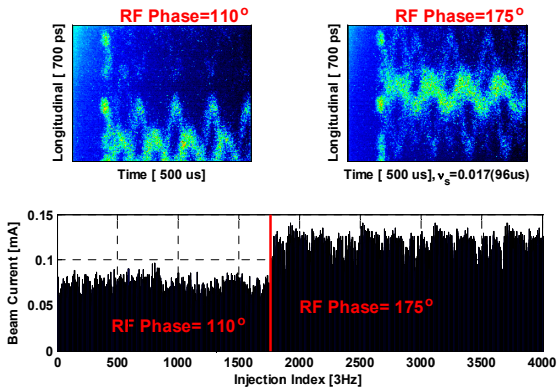

Figure 4: Longitudinal beam motion at the beginning of ramping for varied station phase (top); booster beam current at 3GeV with different RF phase (bottom).

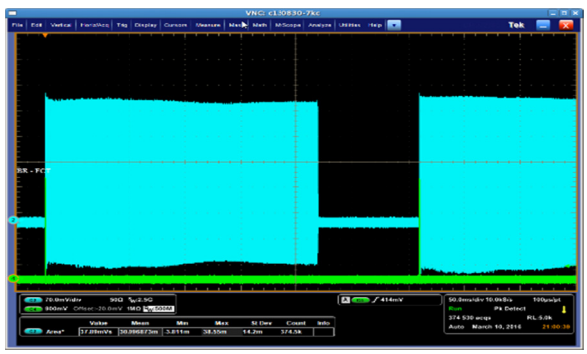

Figure 5: FCT of booster beam current beam during a ramping cycle. Note that energy can be ramped down to 1.3 GeV (260 ms).

EMITTANCE MEASUREMENT

The evolution of the beam emittance and energy spread can be described as following equation [4]:

$$\frac{d\varepsilon_N(t)}{fdt} = -\left[\frac{1}{\gamma(t)}\frac{d\gamma(t)}{fdt} + \frac{2}{f\tau_\infty}\left(\frac{\gamma(t)}{\gamma_f}\right)^3\right]\varepsilon_N(t) + \frac{2}{f\tau_\infty}\left(\frac{\gamma(t)}{\gamma_f}\right)^5 \quad (1)$$

$$\frac{d\sigma_N(t)}{fdt} = \left[\frac{1}{4\gamma(t)}\frac{d\gamma(t)}{fdt} - \frac{1}{f\tau_\infty}\left(\frac{\gamma(t)}{\gamma_f}\right)^3\right]\sigma_N(t) + \frac{1}{f\tau_\infty}\left(\frac{\gamma(t)}{\gamma_f}\right)^7\frac{1}{\sigma_N} \quad (2)$$

in which τ_∞ represents the damping time, γ the Lorentz factor and f the revolution frequency. The beam emittance normalized to the equilibrium state at the final ramping energy (γ_f) is $\varepsilon_N = \varepsilon/\varepsilon_\infty$. In the evolution of beam emittance equation (1), the first two damping terms arise from the adiabatic damping that results from the change of the beam energy and the effect of radiation damping. The last excitation term arises from quantum fluctuation. In equation 2, $\sigma_N = \sigma/\sigma_\infty$ represents the beam energy spread normalized to the equilibrium energy spread (σ_∞) at the final ramping energy (γ_f). The energy spread also damps to an equilibrium state before the beam is extracted.

The evolution of emittance and energy spread due to various terms is shown in Figure 6. A diagnostic system for synchrotron light detection is located at one of photon ports [5]. In this setup, the synchrotron light is captured during the booster ramping. The images are analyzed with a Gaussian fit of the horizontal and vertical projections. The measured sizes of the beam agree satisfactorily with the model values [2].

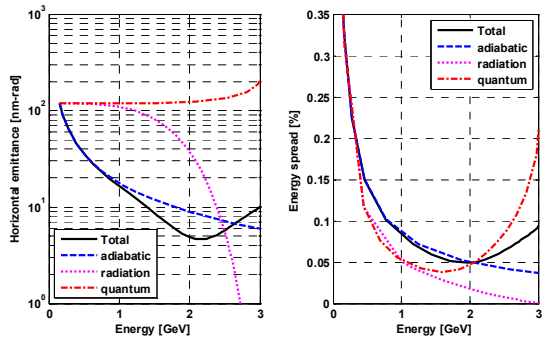

Figure 6: Evolution of beam emittance (left) and energy spread (right) due to various effects.

The horizontal and vertical emittances are deduced from the measured beam sizes σ_x and σ_y according to:

$$\varepsilon_x = \frac{\sigma_x^2 - \eta^2\sigma_E^2}{\beta_x} \; ; \; \varepsilon_y = \frac{\sigma_y^2}{\beta_y} \quad (3)$$

in which the beta function used and the dispersion are given model values, β_x = 3.37 m, β_y = 13.67 m and η_x = 0.248 m. We took the measured energy spread and normalized emittance of the LINAC beam at 150 MeV for the model calculation in Eq. 1 and 2. The energy spread is 0.35 % and normalized emittance ε_{nx} = 36 and ε_{ny} =30 π mm mrad from the LINAC. The evolution of the emittance and energy spread with initial values was computed from the numerical integration of Eq. 1 and 2. The emittance coupling ratio was $\varepsilon_y/\varepsilon_x$ = 0.48 at the equilibrium state. Figure 7 shows comparisons between the emittance measurement and analytical values in both planes. The measured emittances at extraction energy 3 GeV are ε_x=14 nm rad and ε_y=6.8 nm rad.

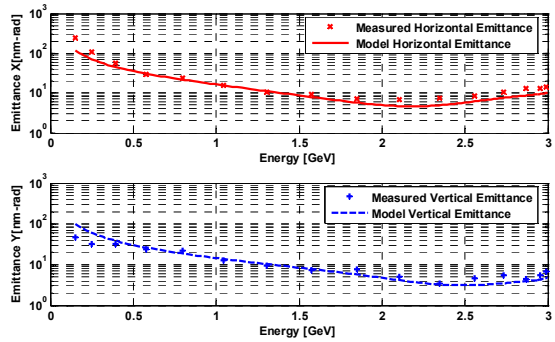

Figure 7: Model and measured emittance evolution in both planes.

LONGITUDINAL BEAM MOTION

The longitudinal beam motion during booster ramp was measured with a streak camera (Hamamatsu C10910).

ISBN 978-3-95450-147-2

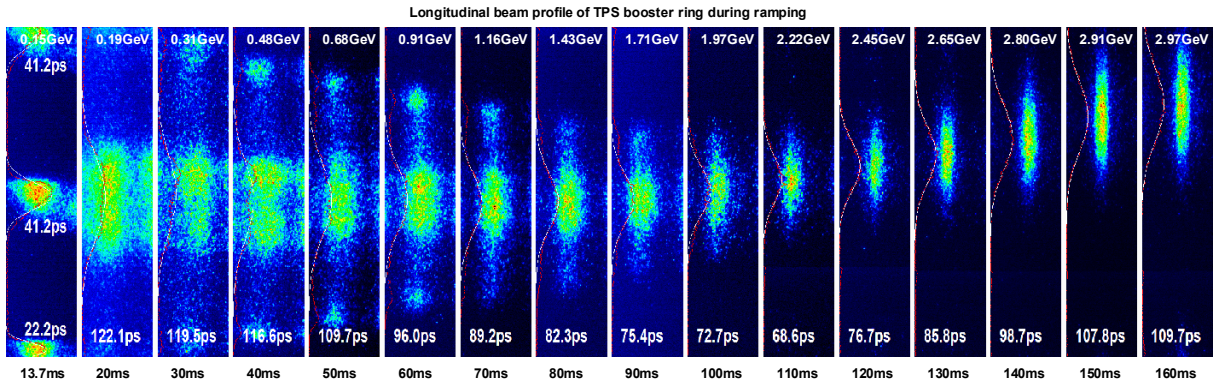

Figure 8: The accumulated longitudinal beam profile and Gaussian fit of the center bunch during ramping.

Figure 8 depicts the variation of accumulated longitudinal motion with energy during ramping. The variation of the length of the main bunch with energy during ramping is completely damped at about 2 GeV or in 100 ms. The length of the main bunch during ramping is shown in Figure 9.

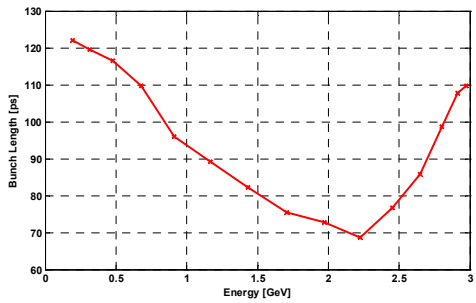

Figure 9: Measured length of main bunch during ramping.

We also observed the movement of synchrotron phase during energy ramping by the streak camera. Figure 10 shows the measured and theoretical values of the synchrotron phase changes along the energy ramping.

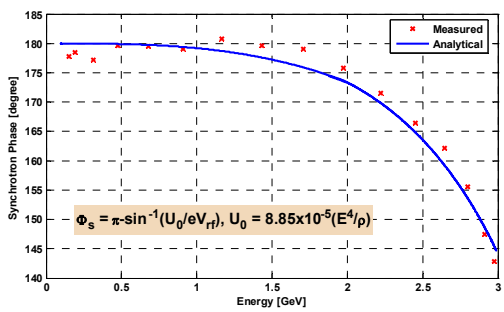

Figure 10: Measured and theoretical value of the synchrotron phase during energy ramping.

Without accumulation, a multi-shot of longitudinal beam motion during 100 ms is shown in Figure 11. The synchrotron oscillations due to the energy vibration are clearly shown. The energy vibration, pulse to pulse, due to the booster dipole power supply offset (±0.2 %) and LINAC (±0.1%) were observed at low energy as shown in Figure 8. The estimated energy vibration was about ~± 0.25% at 20 ms with 100 pixel separation in 300 shots.

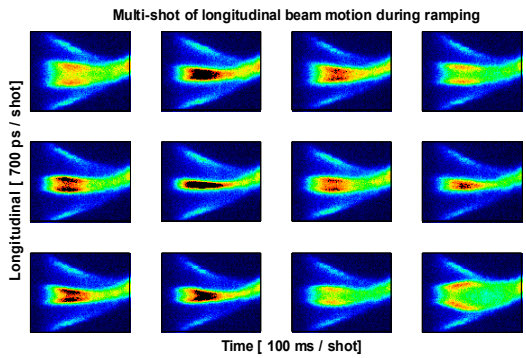

Figure 11: Multi-shot of longitudinal beam motion. The synchrotron oscillation due to the energy variation is observed.

CONCLUSIONS

The TPS booster ring has been optimized for routine operations. The results of measurement of the emittance evolution during ramping in both planes agree satisfactorily with the model values. The longitudinal motion observed with a streak camera reveals the need for further detailed investigation in energy stability.

REFERENCES

[1] C. C. Kuo et al., "Commissioning of the Taiwan Photon Source", *Proc. IPAC'15*, TUXC3, p. 1314.

[2] H. J. Tsai et al., "Hardware Improvements and Beam Commissioning of the Booster Ring in Taiwan Photon Source", *Proc. IPAC'15*, TUPJE053, p. 1741.

[3] M. S. Chiu et al., "Commissioning of Phase-I Insertion Devices in TPS", presented at IPAC'16, Busan, Korea, May 2016, paper THPMB050, this conference.

[4] K. K. Lin et al., "Performance of SRRC 1.3 GeV Electron Booster Synchrotron", Nuclear Instruments & Methods in Physics Research A 361(1995) 1-12.

[5] C. Y. Liao et al., "Preliminary Beam Test of Synchrotron Radiation Monitoring System at Taiwan Photon Source", *Proc. IPAC'15*, MOPTY074, p. 1109.